AIAA/AAS Astrodynamics Specialist Conference and Exhibit
21 - 24 August 2006, Keystone, Colorado

AIAA 2006-6661

The *Actual* Dynamical Environment About Itokawa

D.J. Scheeres[*], R. Gaskell[†], S. Abe[‡], O. Barnouin-Jha[§],
T. Hashimoto, J. Kawaguchi, T. Kubota, J. Saito, M. Yoshikawa[¶],
N. Hirata, T. Mukai[‖], M. Ishiguro[**], T. Kominato, K. Shirakawa[††], M. Uo[‡‡]

The dynamical environment about and on Asteroid 25143 Itokawa is studied using the shape and rotation state model estimated during the close proximity phase of the Hayabusa mission to that asteroid. We first discuss the general gravitational properties of the shape model assuming a constant density. Next we discuss the actual dynamical environment about this body, both on the surface and in orbit, and consider the orbital dynamics of a Hayabusa-like spacecraft. Then we detail one of the approaches used to estimate the mass of the body, using optical and lidar imaging, during the close proximity phase.

I. The Hayabusa Mission and Itokawa

In the Fall of 2005 the Japanese Space Agency's (JAXA) Hayabusa spacecraft had a rendezvous with Asteroid 25143 Itokawa (Fujiwara et al. 2006). In its subsequent mission it stayed in close proximity to the asteroid for three months, during which time it descend to the asteroid surface twice to acquire samples for eventual return back to Earth. Prior to these landings, the spacecraft made a number of trial descents to come close to the surface in order to test its navigation system. During this time period a precise shape model of the asteroid was constructed (Gaskell et al. 2006) which allows for detailed evaluation of the asteroid's surface and close proximity dynamical environment. This shape model is presented in Fig. 1. During one of the trial descents, the spacecraft came within 50 meters of the asteroid surface, providing an opportunity to perform a relatively precise determination of the asteroid's total mass. This opportunity, along with several others, were used to estimate the total mass of the asteroid to be 3.54×10^{10} kg $\pm$ 5% (Abe et al. 2006). This makes Itokawa only the second asteroid for which both a precise shape model and mass are known, after Eros. Thus it is of interest to study the actual surface environment on this body and to evaluate whether it is feasible for a spacecraft to maintain a stable orbit about this body. Also, since the mass determination used a significantly different approach than used previously for an asteroid, it is also important to provide details.

This paper will first discuss the general geometric properties of the Itokawa shape model and its constant density gravity field. Following this, a detailed discussion of the dynamical environment on and about this body will be given, using the data obtained from the Hayabusa spacecraft. In particular, we will compute the surface environment, the dynamics environment close to the body, the dynamics environment far from the body, the effect of solar radiation pressure, and the predicted orbit stability of a Hayabusa-like spacecraft. Following this we will give a more detailed explanation of the mass determination method used for the above mentioned close approach to the asteroid.

[*]Associate Professor, The University of Michigan, Department of Aerospace Engineering, Ann Arbor, MI 48109-2140 USA, 1-734-615-3282 (tel), 1-734-763-0578 (fax), scheeres@umich.edu
[†]JPL/Caltech, Pasadena, CA, USA
[‡]Univ. of Kobe, Japan
[§]JHU-APL, USA
[¶]JAXA-ISAS, Japan
[‖]Univ. of Aizu, Japan
[**]Seoul University, Korea
[††]NEC Aerospace, Japan
[‡‡]NEC-Toshiba Space Systems, Japan

II. Computed properties from the shape and total mass

Given the measured mass, the total gravitational parameter μ of Itokawa equals: $2.36\times10^{-9}\pm0.15\times10^{-9}$ km^3/s^2. The total volume of the measured shape model is 1.78×10^{-2} km^3. Combining these we have a bulk density for the asteroid of 1.98 g/cm^3, with some associated error.

Given the detailed polyhedral shape of Itokawa we can compute a variety of quantities associated with that body. For all our discussions we assume a body-fixed coordinate frame with origin at the body center of mass and aligned with the principal axes of inertia of the asteroid (all computed assuming a uniform density throughout). We adopt the usual convention that the x axis is along the smallest moment of inertia (longest axis), the z axis is along the largest moment of inertia (shortest axis), and that the y axis lies along the intermediate moment of inertia. Also, where applicable, we have assumed that the body rotates about its maximum moment of inertia (consistent with observations taken during the mission) with a rotation period of 12.132 hours.

The overall dimensions of the asteroid shape in each of the principal directions are:

$$\begin{aligned} x &: -0.2532 \rightarrow 0.3026 \\ y &: -0.1531 \rightarrow 0.1496 \\ z &: -0.1190 \rightarrow 0.1240 \end{aligned}$$

with overall lengths of 0.5558, 0.3027, and 0.2430 km in the x, y, and z directions, respectively. Note, these overall lengths measure the maximum difference between coordinate values for the shape. The total surface area of the asteroid is 0.395 km^2, and the total volume of the asteroid is 1.78×10^{-2} km^3. Associated with the volume is the mean radius of the body, $r_M = 0.1620$ km, defined as the radius of a sphere with equivalent volume.

The higher-order mass distributions of the body, which include the inertia moments and the gravitational coefficients up to an arbitrarily high order, can be computed using the methodology outlined in Werner (1997). We find the moments of inertia:

$$\begin{aligned} I_x/M &= 0.637 \times 10^{-2} \text{ km}^2 \\ I_y/M &= 2.122 \times 10^{-2} \text{ km}^2 \\ I_z/M &= 2.235 \times 10^{-2} \text{ km}^2 \end{aligned}$$

where we quote the moments of inertia divided by the total mass of the body. From the moments of inertia we can solve for the ellipsoid with the same moments of inertia, and we find a body with semi-major axes of $0.3049 \times 0.1369 \times 0.1144$ km, which deviate from the overall dimensions of the body, probably due to the large concavity in the neck region of Itokawa (see Fig. 1). Directly related to moments of inertia are the second degree and order gravity coefficients. These are directly computed to be:

$$\begin{aligned} C_{20}R_s^2 &= -8.513 \times 10^{-3} \text{ km}^2 \\ C_{22}R_s^2 &= 3.713 \times 10^{-3} \text{ km}^2 \end{aligned}$$

where R_s is the arbitrary normalization radius. A gravity field expanded to degree and order 4 is given in the Appendix; a higher order gravity field can be obtained from the author on request. A simple measure of the asteroid's shape and gravity field with dynamical implications is defined in Hu and Scheeres (2004) as:

$$\sigma = \frac{I_y - I_x}{I_z - I_x} \tag{1}$$

For Itokawa this value is $\sigma = 0.93$. A body with $\sigma = 1$ has a prolate inertia matrix while one with $\sigma = 0$ has an oblate matrix, thus we see that Itokawa is very close to having a prolate shape index.

III. Derived dynamical properties for surface, close proximity, and vicinity motions

Under the constant density assumption a number of dynamical constraints for natural and spacecraft motion about Itokawa can be placed on the surface environment, the close proximity dynamical environment, and the environment in the vicinity of Itokawa, where solar perturbations become relevant.

Figure 1. Shape of the Itokawa model showing, starting clockwise from the top, the North pole, equatorial view from 90° East, view from 270° East, South pole, equatorial view from 180° East, and view from 0° East (Gaskell et al. 2006).

A. Surface Environment

Following the methodology outlined in Scheeres et al. (1996), we compute the apparent slope over the surface of the asteroid, the total gravitational plus centripetal accelerations over the body, and the necessary and sufficient speeds for ejecta to escape from the asteroid. Itokawa has slopes ranging up to a maximum of

69° in some regions, above the traditional angle of repose for a granular material. The average slope over the body is a relatively subdued 13° and 95% of the body has slopes less than 30°. Fig. 2 shows the slope distribution mapped onto the Itokawa shape model and Fig. 3 the slope distribution.

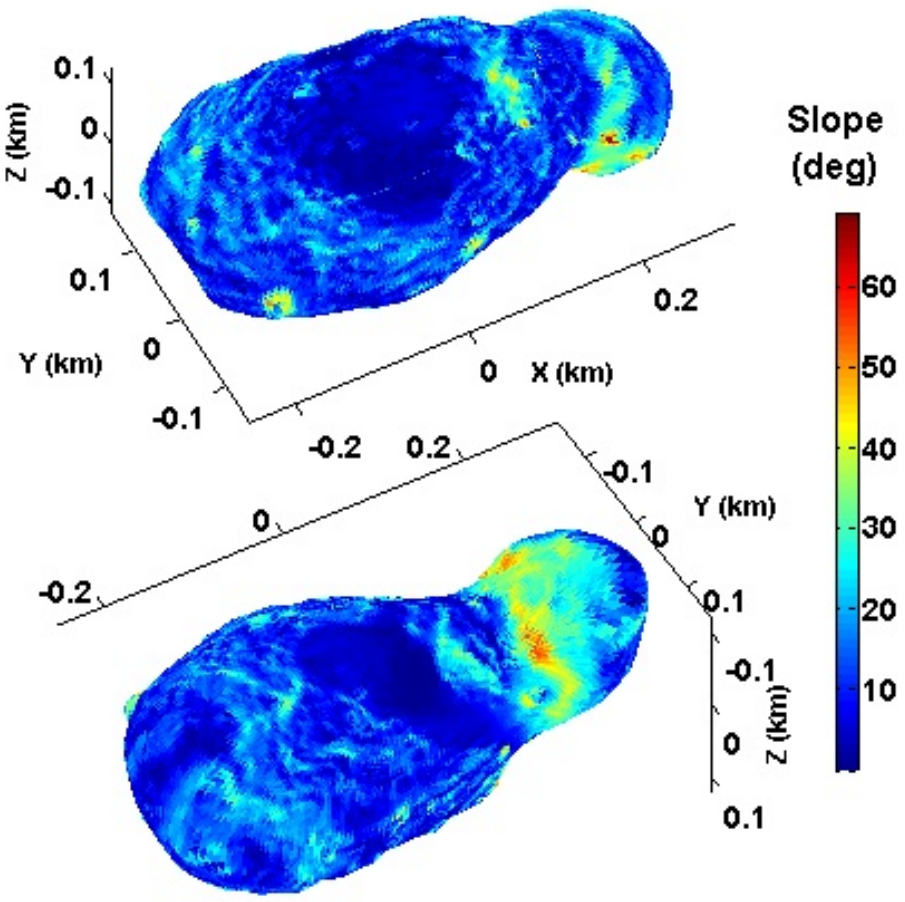

Figure 2. Slope values mapped onto the surface of the Itokawa model (Fujiwara et al. 2006).

The maximum total surface acceleration (combining gravitational and rotational accelerations) is 0.086 mm/s^2 and the minimum is 0.056 mm/s^2, for a variation of 54% from minimum to maximum. These accelerations can also be broken into components normal to the local surface and tangential to the local surface. These distinctions are important when electrostatic forces and the sliding motion of particles are considered. The accelerations normal to the surface range from 0.024 $\rightarrow$ 0.086 mm/s^2. The accelerations tangent to the surface range from $\sim 0 \rightarrow$ 0.062 mm/s^2.

The surface environment can also be described by defining the necessary and sufficient surface launch speeds for escape from the asteroid (neglecting solar perturbation effects). The necessary launch speeds are the absolute minimum speed a particle must have if it is to escape from the asteroid, i.e., any launch speed less than this ensures that the particle will not leave the asteroid and will reimpact at some point in the future. These necessary speeds range from 0.08 $\rightarrow$ 0.13 m/s over Itokawa's surface. The sufficient launch speeds, on the other hand, are speeds that ensure that a particle launched with this speed in a direction normal to the surface will escape from the asteroid. These speeds range from 0.11 $\rightarrow$ 0.23 m/s over the surface and are shown in Fig. 4. At each point of the asteroid, values between these speeds define launch speeds where the final evolution is not known. The differences between these speeds range from 0.03 $\rightarrow$ 0.10 m/s.

In addition to bulk surface properties for Itokawa, such as slope, the local topology and direction of slope vectors are also of importance for understanding the surface properties of the body, distribution of regolith, and to plan the motion of a surface vehicle. In Fig. 5 we show a view of the Itokawa surface with the slope

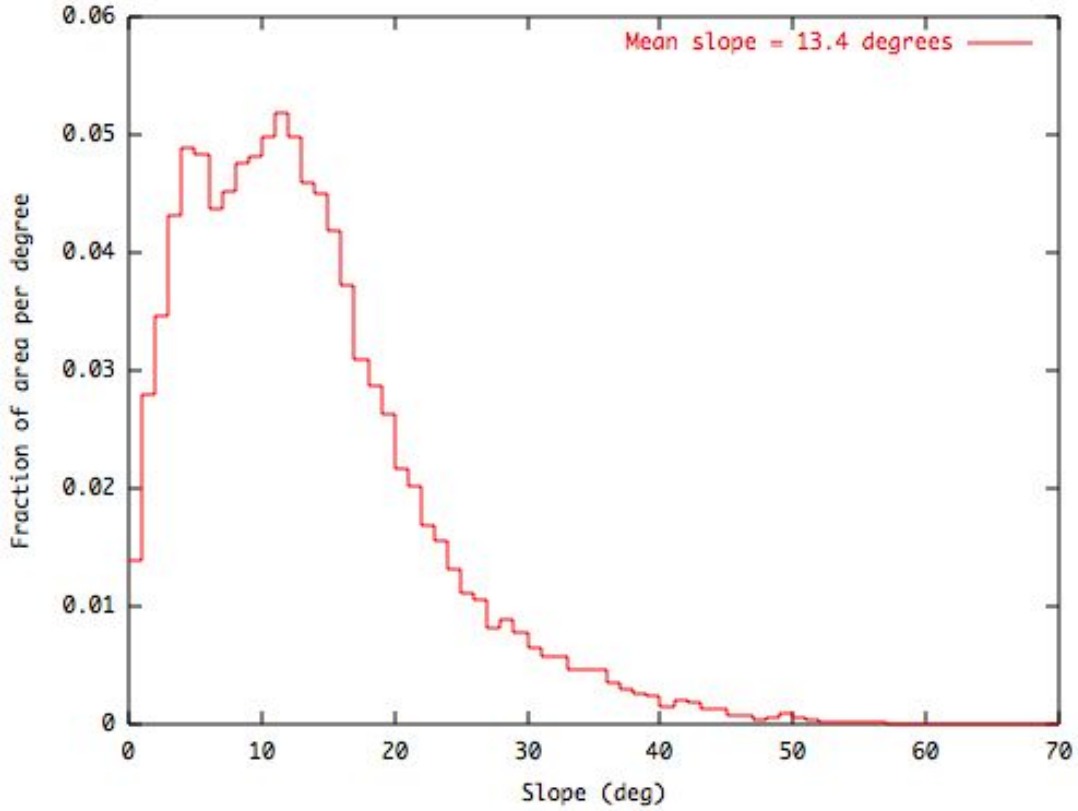

Figure 3. Slope distribution over Itokawa.

vector distribution, which plots the slope in color on the surface and superimposes the direction in which the acceleration tangent to the surface points. On Itokawa there are strong correlations between these slope directions and the apparent downslope motion of material. The potential minimum on the surface is located in the polar regions and along the asteroid neck, which is also where all the fine material on the asteroid is found. Figure 6 shows the relative geopotential of Itokawa.

B. Gravitational Dynamical Environment

First we evaluate the dynamical environment close to Itokawa neglecting the solar radiation pressure and solar gravity perturbations. This neglect is not valid for the Hayabusa spacecraft, for which the effect of solar radiation pressure must be accounted for, even for motion close to the body. Thus, the results in this section only apply to larger natural particles with size greater than ~ 10 centimeters, such as ejecta blocks which may be lofted into orbit about Itokawa following an impact.

The simplest parameterization of the close proximity dynamical environment can be made by computing the "resonance radius" of the body, which we define as the distance at which the point mass gravitational attraction of the body equals the centripetal acceleration due to the rotation of the asteroid. This is computed as $r_{res} = \left(\mu/\omega^2\right)^{1/3}$, where ω is the rotation rate of Itokawa, equal to 1.4386×10^{-4} rad/s. For Itokawa this radius is $r_{res} = 0.485$ km.

A more precise measure of the close proximity environment can be found by computing the orbits synchronous with the rotating body (Scheeres 1994, Scheeres et al. 1996). For a near-ellipsoidal body such as Itokawa there will only be four such points, corresponding to true circular orbits about Itokawa with

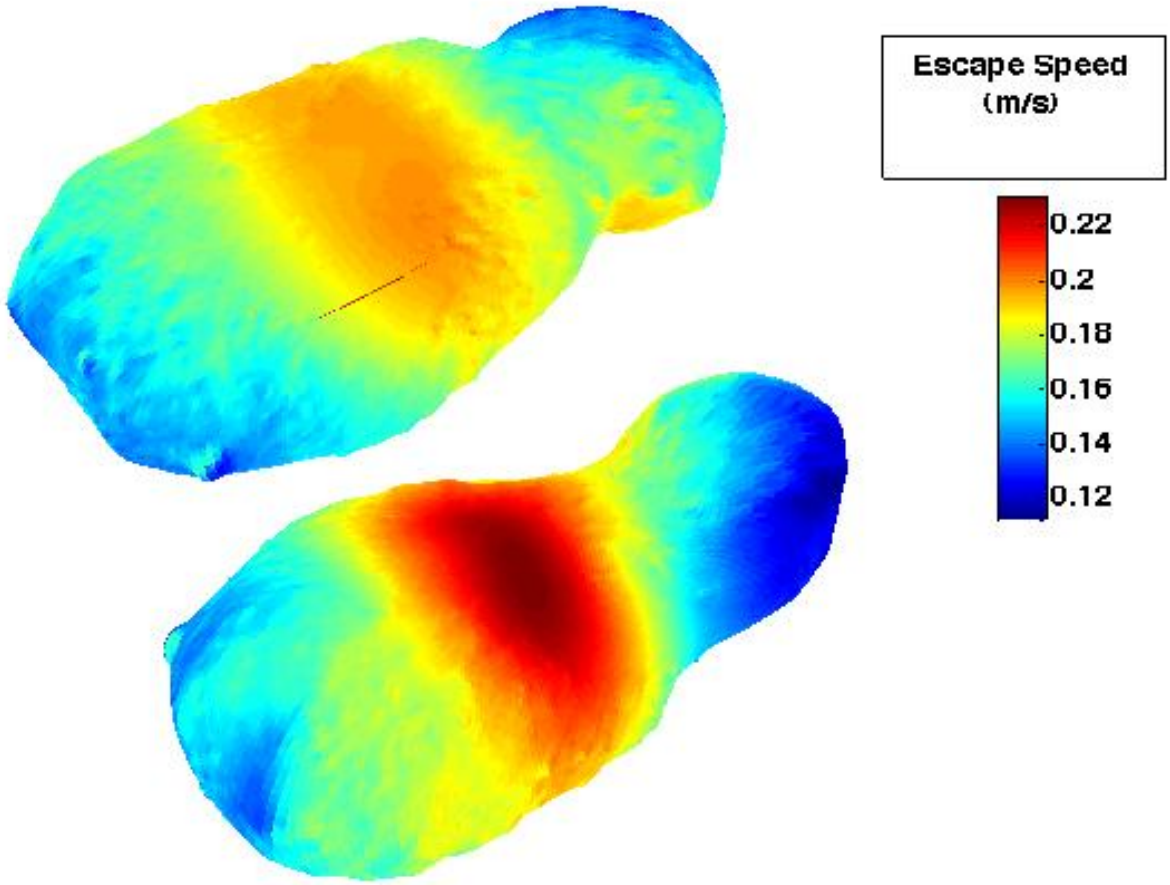

Figure 4. Sufficient escape speeds over Itokawa.

orbit period exactly equal to the Itokawa rotation period. These orbits appear as equilibrium points in the equations of motion about the asteroid when stated in the body-fixed (i.e., rotating) frame. Thus, their coordinates can be given in the body-fixed coordinate frame (x, y, z):

$$
\begin{aligned}
E_1: &\quad 0.5205, 0.0173, -0.0084 \text{ km} \\
E_2: &\quad 0.0325, 0.4692, 0.0019 \text{ km} \\
E_3: &\quad -0.5121, 0.0231, -0.0043 \text{ km} \\
E_4: &\quad 0.0341, -0.4719, 0.0015 \text{ km}
\end{aligned}
$$

Figure 7 shows the location of these points in the Itokawa-fixed frame. The stability of these equilibrium points has been computed and we find that all four are unstable, making this a "Type II" asteroid (applying the criterion from Scheeres 1994). The points E_1 and E_3 have a simple hyperbolic unstable manifold with characteristic times (i.e., time for an initial error to grow by a factor of 2.7) of 2.4 and 3.0 hours, respectively. There are also two oscillation frequencies about each of these equilibrium points, with periods of ~ 11 hours. The points E_2 and E_4 are complex unstable with characteristic times of 5.6 and 6.6 hours, respectively, with an associated period of ~ 16 hours for the spiral motion. All the equilibrium points have an additional oscillation mode in the direction parallel to the rotation pole with a period of ~ 12 hours. The presence of four unstable orbits indicates that motion in close proximity to Itokawa will be subject to destabilizing influences from the gravity field, the exception being retrograde orbits with high inclinations (on the order of $135^\circ \rightarrow 180^\circ$), which is expected from the theory of asteroid orbiters (Scheeres et al. 2000).

In Hu and Scheeres (2004) a non-dimensional parameter that serves as a combined measure of the effect of asteroid gravity and rotation rate is defined, $(I_z - I_x)\sigma/r_{res}^2$, with a value of ~ 0.063 for Itokawa. Using

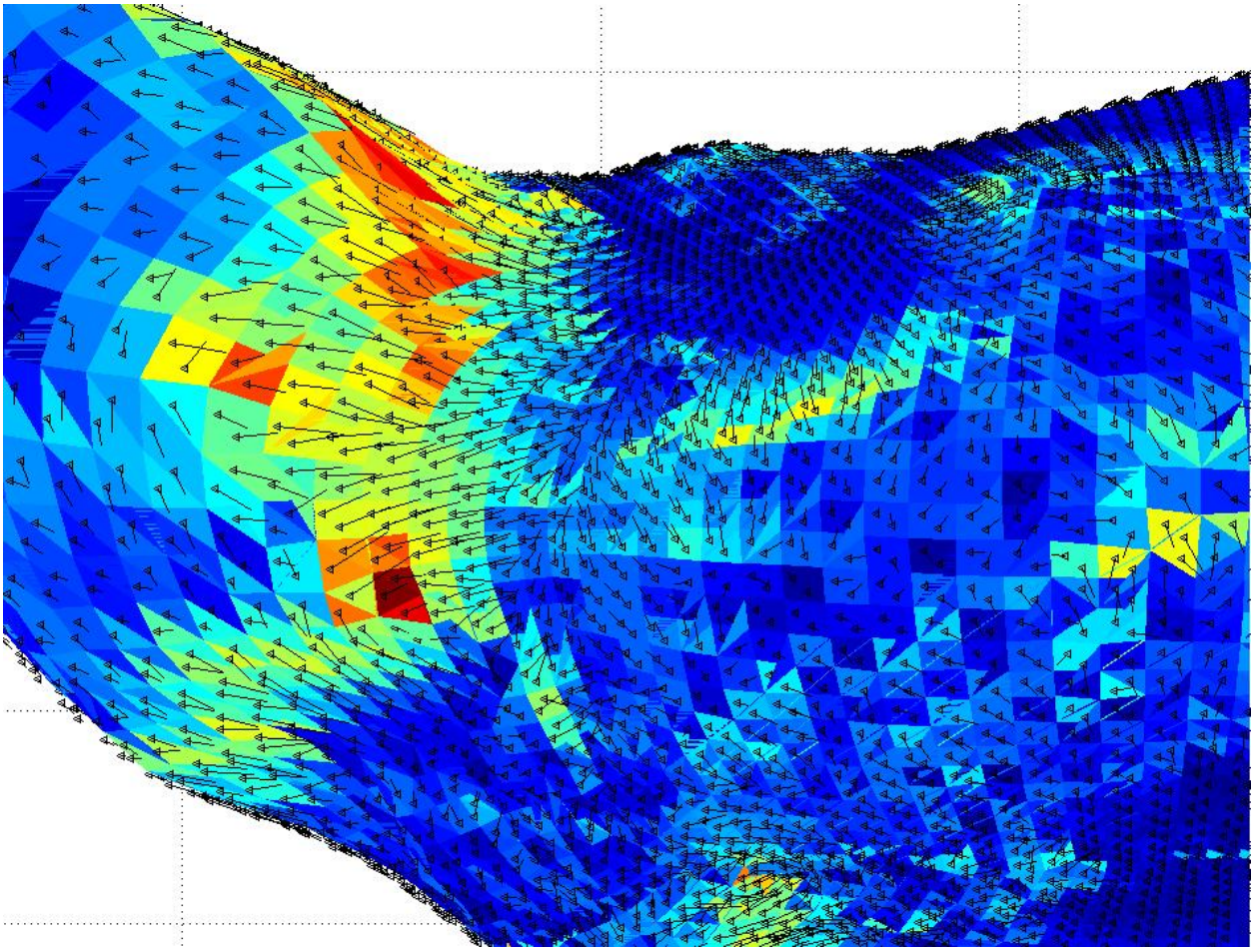

Figure 5. Slope vectors on the Itokawa shape model. Note that the vectors converge towards the visible Itokawa pole in this figure.

the results from Hu and Scheeres (2004), we estimate that near-circular, direct orbits will be stable out to a distance of $\sim 2.5^{2/3} r_{res}$ from the center of Itokawa, which corresponds to an orbit radius of 0.9 km (see Fig. 7). We note that this is an approximate limit only and that motion outside of this radius may still be subject to destabilizing interactions through higher-order resonances.

C. Gravitational plus Solar Dynamical Environment

Next we discuss the dynamical environment further from the asteroid, in the realm where solar gravity and radiation pressure begin to dominate the motion of ejecta and spacecraft. We can split this discussion into two parts, the effect of solar gravity on motion about the asteroid and the combined effect of solar gravity and radiation pressure on motion. We note that for motion of larger ejecta, it is sufficient to only consider solar gravity, however for the motion of small ejecta or a spacecraft solar radiation pressure dominates over solar tide.

The effect of solar gravity can most easily be delimited in terms of the Hill sphere about the asteroid. Since Itokawa is in an elliptic orbit about the sun (perihelion radius of 0.953 AU and aphelion radius of 1.69 AU), the size of the Hill sphere will fluctuate and can be computed to be:

$$R_{Hill} = d\left(\frac{\mu}{3\mu_S}\right)^{1/3} \tag{2}$$

where μ is the asteroid gravitational parameter, μ_S is the gravitational parameter of the sun, and d is the distance between the asteroid and sun. For Itokawa we find that the Hill radius will vary between 25 km at

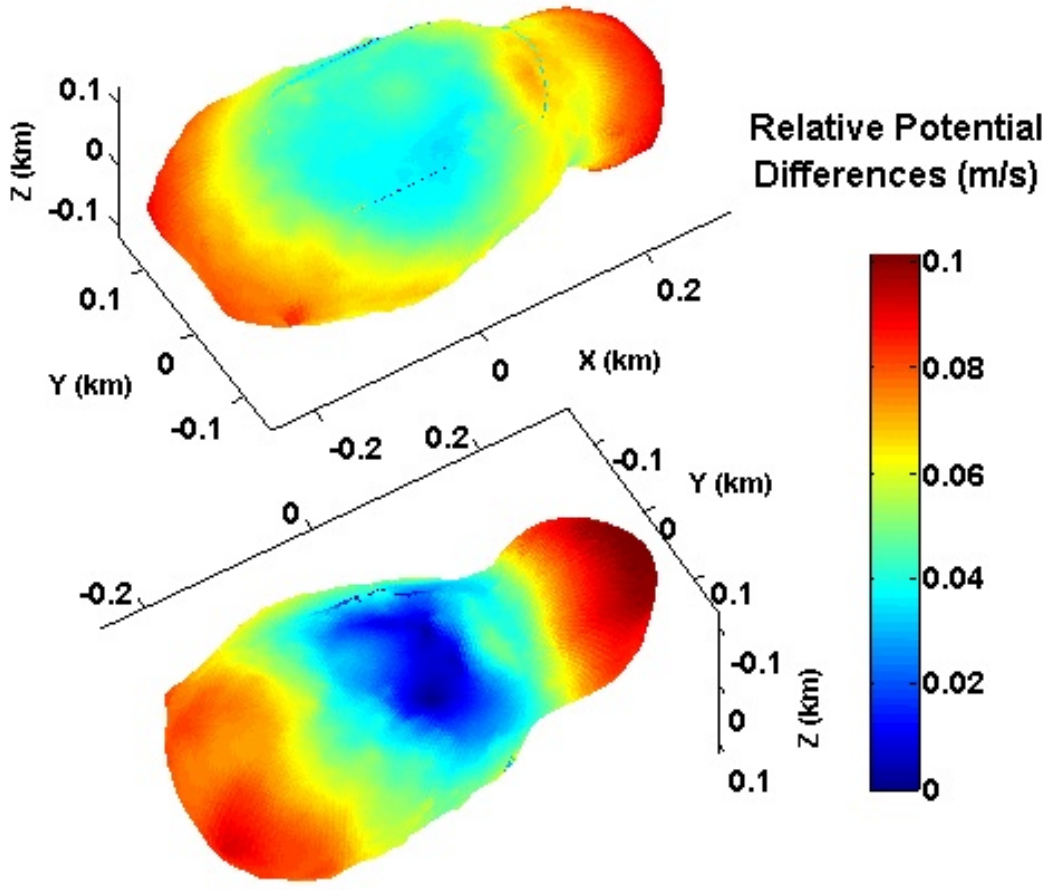

Figure 6. Gravitational plus rotational potential mapped onto the surface of the Itokawa model (Fujiwara et al. 2006). This plot measures the speed needed to energetically transition from the lowest potential point on Itokawa to any other region. Conversely, it measures the speed a particle dropped with zero speed at that location if it fell unimpeded to the lowest potential point on Itokawa, which is situated within the Muses Sea Region. Upper view shows the Northern hemisphere, lower view the Southern hemisphere.

perihelion and 45 km at aphelion. Using the analysis from Scheeres and Marzari (2002) we estimate that the semi-major axis of orbits which remain bound to the asteroid for at least several particle orbits range from 10.2 → 18.2 km (the limits corresponding to perihelion and aphelion). These limits are well outside the limiting radius for strong interactions with the asteroid gravity field, but are only valid for a body insensitive to solar radiation pressure.

To include the effect of solar radiation pressure, it is necessary to specify the mass to projected area ratio of the object orbiting about the asteroid. The relevant parameter that describes the relative strength of the solar radiation pressure force is defined in Scheeres and Marzari (2002) as $\tilde{\beta} = 3.84/B/\mu^{1/3}$, where B is the mass to area ratio of the orbiting body in kg/m^2, and μ is the gravitational parameter of the asteroid. When $\tilde{\beta} \ll 1$ the solar radiation pressure effect is small, but when it is equal to or greater than 1 its effect will be quite strong. For a spherical body with an assumed density of 4 g/cm^3, an object with radius 50 cm will have a $\tilde{\beta} = 1$ and a mass to area ratio $B = 2884$ kg/m^2.

The estimated mass to projected area ratio of the Hayabusa spacecraft was approximately ~ 30 kg/m^2. This leads to a solar radiation pressure parameter $\tilde{\beta} \sim 96$, indicating that this force will be very relevant. As described in Scheeres and Marzari (2002), the Hill region is no longer spherical but is highly skewed away from the asteroid on the sun-side and towards the asteroid on the anti-sun side. For the Hayabusa spacecraft the sun-side libration points range between 1078 → 1912 km, while the anti-sun-side libration points range between 5.2 → 9.2 km. We note the large disparity between these limits. Due to solar radiation pressure, the semi-major axis for the sufficient condition for the spacecraft to be bound to the asteroid over several

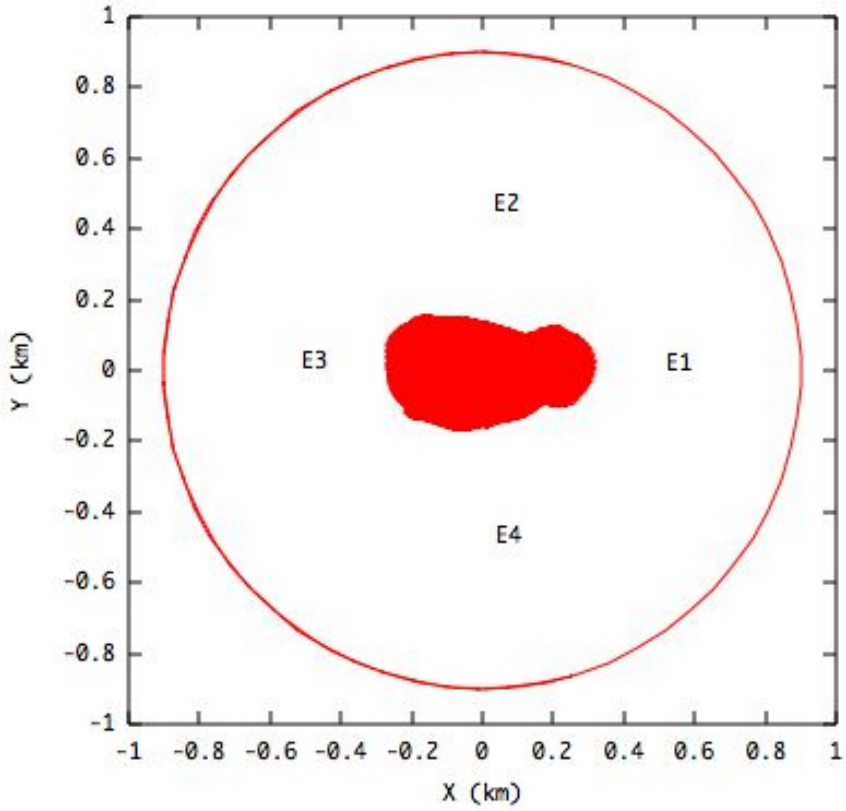

Figure 7. Pole-on view of Itokawa with locations of the equilibrium points indicated and the approximate stability limit for direct orbits marked with a circle.

orbits ranges from 1 → 1.75 km. All the limits in the above ranges correspond to perihelion and aphelion. The numerically determined limit for the spacecraft to be bound to the asteroid, assuming an initial orbit in the sun terminator plane, is found to be 1.75 km at perihelion, although the orbit is only loosely bound at this limit.

We can also use these limits to predict the smallest sized regolith grains on the surface of Itokawa. As is currently suspected, small particles on asteroid surfaces will be subject to levitation forces due to the plasma environment on their surface (Lee 1996, Robinson et al. 2001). When such levitation occurs on a small asteroid, the particles can be placed into orbit and may potentially escape if the solar radiation pressure acceleration is larger than the surface acceleration. For Itokawa, particles with a mass to area ratio less than 5.7×10^{-3} g/cm^2 are susceptible to being swept off of the surface. If we assume the particle is a sphere with density 4 g/cm^3 this corresponds to particle sizes of 10 microns. If particles are subject to levitation on the order of tens of meters or higher, the particle size that can be swept away grows significantly. The solar radiation pressure also means that particles can more easily escape from the asteroid if given an initial surface ejection speed, as a positive semi-major axis can still lead to escape. Applying this effect to the previously described sufficient escape speed, we find that particles of size 1 mm have escape speeds over the surface of 0.08 → 0.22 m/s, while particles of size 0.1 mm have escape speeds ranging over 0 → 0.19 m/s, evaluated at perihelion. Thus, we expect the surface of Itokawa to be depleted at the smallest particle sizes, consistent with observations of the Itokawa surface (Yano et al. 2006). Analysis of the sample return canister upon return to the Earth may further elucidate these minimum limits.

D. Stability of spacecraft trajectories

This analysis also predicts that the Hayabusa spacecraft's trajectory will be strongly perturbed by the solar radiation pressure. It is important to note that the Hayabusa used a "hovering" approach to their vicinity operations. Despite this, it is of interest to explore whether the Hayabusa spacecraft could have entered a stable orbit about Itokawa, as future missions may be interested in adopting such an approach.

First we note some particular facts concerning orbital motion in the presence of strong solar radiation pressure perturbation. All motion that occurs in the asteroid orbital plane will have a strong tendency for eccentricity to approach unity due to solar radiation pressure, while the semi-major axis remains constant (Scheeres 1999). Thus, such orbits tend towards impact trajectories. In general, as the spacecraft orbit inclination relative to the asteroid orbital plane increases, an evolving orbit will reach a maximum eccentricity less than unity. Still, these orbits tend to be unsafe, as any increase in eccentricity allows the trajectory to interact more strongly with the rotating Itokawa gravity field. This eccentricity oscillation effect diminshes until the orbit inclination relative to the asteroid orbit plane is 90°, with the orbit oriented so that it lies in the sun-terminator plane. This configuration results in a stable sun-synchronous orbit, and variations in the orbit eccentricity can be minimized. The most stable configuration for these orbits is designed as follows. The eccentricity of the orbit is chosen according to the rule:

$$e = \frac{1}{\sqrt{1+\Lambda^2}} \tag{3}$$

$$\Lambda = 18.9\sqrt{a} \tag{4}$$

where a is the semi-major axis in km and the parameter Λ is evaluated for the Itokawa and Hayabusa parameters using the general formula given in Scheeres (1999). Thus, for an orbit with semi-major axis of 1 km, an eccentricity of 0.05 is prescribed. For this eccentricity to minimize the variations also requires that the periapsis be oriented directly (90 degrees) below the orbit plane if the orbit angular momentum points away from the sun, and directly above the orbit plane if this orbit angular momentum points towards the sun. It is in general sufficient to just start the spacecraft trajectory in the sun terminator plane with a zero eccentricity and the resulting trajectory will have oscillations in eccentricity on the order of 0.1 for a 1 km orbit.

It is important to note that our numbers give a formal prediction of a "stability" interval about the asteroid for the Hayabusa spacecraft, between the capture radius for solar radiation pressure and the lower bound on stable, near-circular motion. Also, although we have predicted the existence of stable retrograde orbits about this mass distribution. These results should be treated with caution, however, as there are non-trivial interactions between the solar radiation pressure and gravitational field perturbations of Itokawa.

To properly consider the interactions between the solar effects and the Itokawa gravity field we need to specify the asteroid's orbit in a frame oriented along its rotation pole. This is the natural frame in which to discuss orbit dynamics, as close proximity motion to the body is fundamentally organized by its rotation pole, and the preferred sun-terminator planes for motion more distant from the body need to be understood in this same reference frame. Based on measurements taken during the rendezvous phase we use an obliquity of 178° (Demura et al. 2006). Thus, sun-terminator orbits at Itokawa will have an inclination in the Itokawa-based frame of almost 90°, which is fortuitous as a larger or smaller inclination can cause the orbit plane to precess independent of the sun-synchronous motion of the asteroid about the sun due to the effect of the asteroid oblateness, which can cause orbital instability. Indeed, we find that sun-terminator orbits of a Hayabusa spacecraft model at Itokawa remain stable and sun-synchronous for larger semi-major axes up to orbit radii of 1.5 km at perihelion (Figs. 8, 9). We find that such orbits are the only feasible ones for motion about Itokawa. At semi-major axes lower than 1.0 km, we find that the asteroid 2nd degree and order gravity field causes precession effects to become strong enough to force the trajectory to rotate out of the terminator plane, which in turn causes the orbit to become unstable (Fig. 10).

For the Hayabusa spacecraft we find that retrograde orbits, which are extremely stable against gravitational perturbations, can become destabilized due to the solar radiation pressure. This occurs as retrograde orbits lie close to the orbital plane, and hence the solar radiation pressure effect forces them to a unity eccentricity. This effect can be partly mitigated, however, for close orbiters as the gravity field will cause their argument of periapsis to have a large precession rate (Scheeres 1994), which will limit the maximum eccentricity which retrograde orbits reach. The combined effect of these perturbations causes the eccentricity to go through large variations, but not as large as if the central body were a simple sphere. Thus, we find it feasible to place the Hayabusa spacecraft in a retrograde orbit, although the necessary radius of these orbits

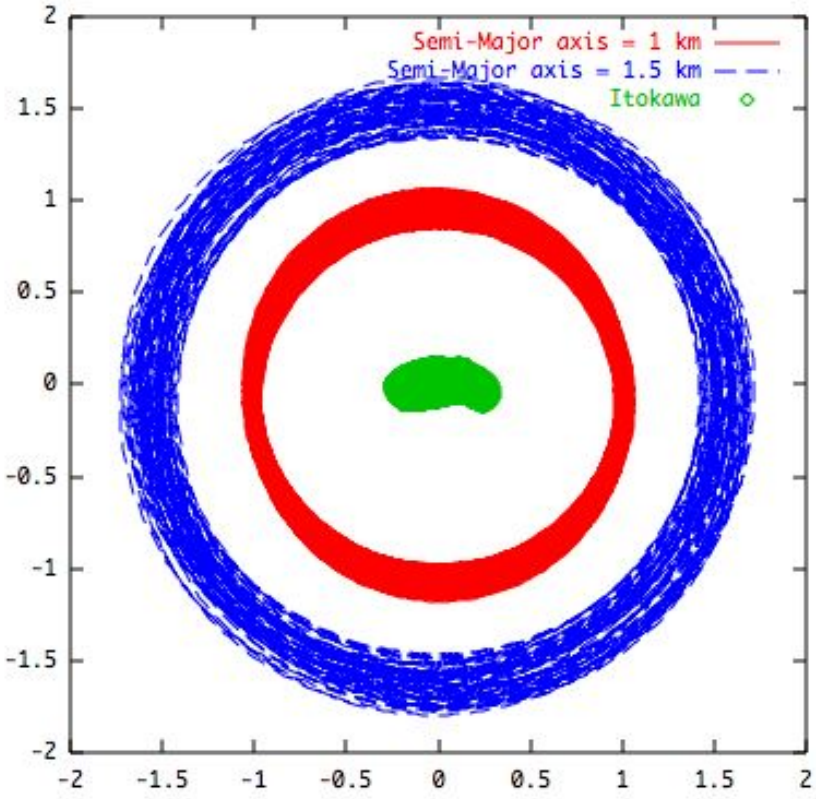

Figure 8. Integrated orbits of Hayabusa about Itokawa in the sun-terminator plane showing the limiting semi-major axes for stable orbits that persist for over 6 months, 1.0 and 1.5 km. Viewed from the sun.

are very close to the surface (within 0.5 km of the center of mass) and are very susceptible to orbit injection errors.

IV. Estimation of the Itokawa gravity

Finally, to end this paper we provide a detailed explanation of the approach used to make one of the estimates of the total mass of the asteroid (Yoshikawa et al. 2006). The estimate in question used the closest approach data available during which ballistic arcs were present along with sufficient images of the asteroid surface taken from within a few hundred meters. This opportunity occurred during the November 12 trial descent to the surface. Figure 11 shows the trajectory from which this determination was made, and also shows the relative location of the spacecraft where images of the asteroid were obtained. We note that the mass determination followed a much different approach used for the asteroid Eros (Miller et al. 2002). This was dictated by the unique trajectory of the Hayabusa spacecraft, which never went into orbit about the asteroid for any length of time.

A. Dynamical Model

Due to the close proximity of the spacecraft to the asteroid during this descent we used a reference frame fixed in the Itokawa frame. Thus, the equations of motion of the spacecraft included Coriolis and centripetal acceleration terms due to the rotation of the asteroid. As the total time span of the reference trajectory was

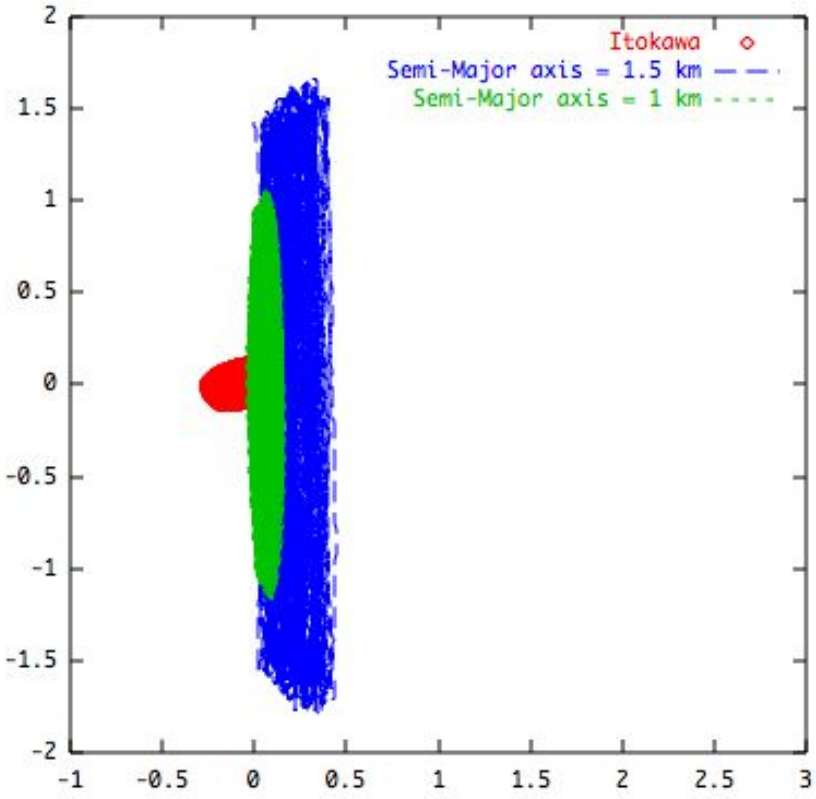

Figure 9. Integrated orbits of Hayabusa about Itokawa in the sun-terminator plane showing the limiting semi-major axes for stable orbits that persist for over 6 months, 1.0 and 1.5 km. Trajectory viewed from above the orbit plane, sun off along the negative horizontal axis.

on the order of 3 hours these accelerations were important, as the asteroid rotated through a full 90° during this time. The specific equations of motion used were:

$$\ddot{\mathbf{r}} + 2\omega\hat{\mathbf{z}} \times \dot{\mathbf{r}} + \omega^2\hat{\mathbf{z}} \times (\hat{\mathbf{z}} \times \mathbf{r}) \quad = \quad \frac{\partial U}{\partial \mathbf{r}} + \mathbf{a} + \sum_i \mathbf{T}_i \tag{5}$$

where $\mathbf{r}$ is the position vector of the spacecraft in the asteroid-fixed frame, $\dot{\mathbf{r}}$ and $\ddot{\mathbf{r}}$ denote velocity and acceleration relative to the asteroid-fixed frame, respectively, ω is the rotation rate of Itokawa, $\hat{\mathbf{z}}$ is the unit vector along the axis of maximum moment of inertia of the Itokawa shape model, U is the gravitational force potential for Itokawa, $\mathbf{a}$ is the solar radiation pressure acceleration acting on the spacecraft and $\mathbf{T}$ are the impulsive thrusts that acted on the spacecraft. A detailed derivation and description of these equations can be found in (Scheeres et al. 2000).

The force potential U was determined directly from the estimated shape model of the asteroid, presented in Fig. 1 (Gaskell et al. 2006) using the polyhedral gravity model (Werner and Scheeres 1996). This model assumes constant density, but fully accounts for the mass distribution of the body. Future research may revisit these results to determine if any detectible non-homogeneities exist in the mass distribution. Although extremely high resolution versions of the Itokawa shape model exist, the effect of small scale mass distribution effects do not influence the total mass distribution in a measurable way. Thus, our orbit computations used a model with modest shape resolution, dividing the surface into 13,000 facets, each having an area of 30 m^2 on average. This is more than sufficient accuracy for the current purposes.

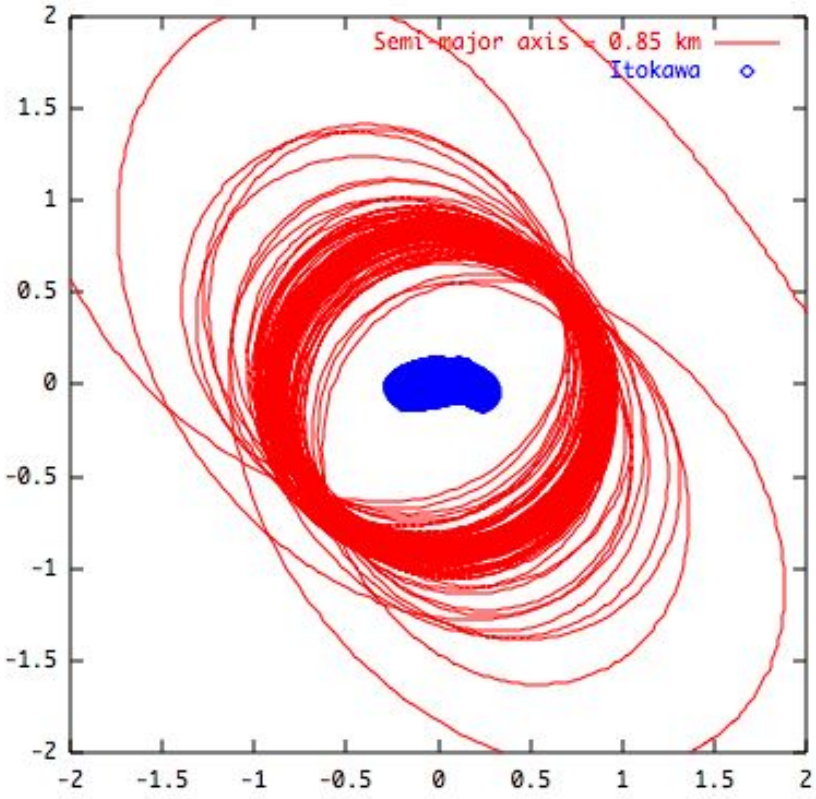

Figure 10. Integrated orbit of Hayabusa about Itokawa in the sun-terminator plane for an initial semi-major axis of 0.85 km. This is small enough to enable destabilizing interactions between the gravity and solar radiation pressure effects. The trajectory eventually escapes from the asteroid.

The solar radiation pressure acceleration **a** was computed assuming the spacecraft is a flat plate with mass to area ratio of 33 kg/m^2. It is important to note that during the flyover the spacecraft was always well within 1 km from the asteroid center of mass. Comparing the total solar radiation pressure acceleration ($\sim 1.5 \times 10^{-10}$ km/s^2) with the total gravitational attraction at 1 km ($\sim 2.36 \times 10^{-9}$ km/s^2) we find that at these close distances the solar radiation pressure is only 6% of the gravitational attraction, decreasing to 0.4% at closest approach. Given the level of uncertainty in our mass determination, we see that the effect of the solar radiation pressure was marginal at best. Thus, although we had the ability to formally estimate the effect of the solar radiation pressure on the trajectory through a scale factor, we did not do this in practice as earlier test runs showed that this was not necessary.

The influence of spacecraft thrusting events were significant. During the time span modeled there were 11 distinct maneuvers performed large enough to have an influence on the trajectory. Such maneuvers inject a large amount of noise into the trajectory and also have a significant influence on changes in the trajectory. To enable this estimation process to work required that, first of all, we have relatively precise estimates of the maneuver times and magnitudes. These were obtained from the Hayabusa navigation team and used as inputs to our estimation routine. These maneuver estimates were themselves somewhat uncertain, due in part to calibration errors in the thrusters that arose from the drastically changing thermal environment of the spacecraft when it came in close proximity to the asteroid. Additionally, these were finite burns but were treated as impulsive burns in our model, a source of additional error. Thus we found it essential to also estimate the maneuver vectors and the time of maneuver in the filter, although the *a priori* uncertainties

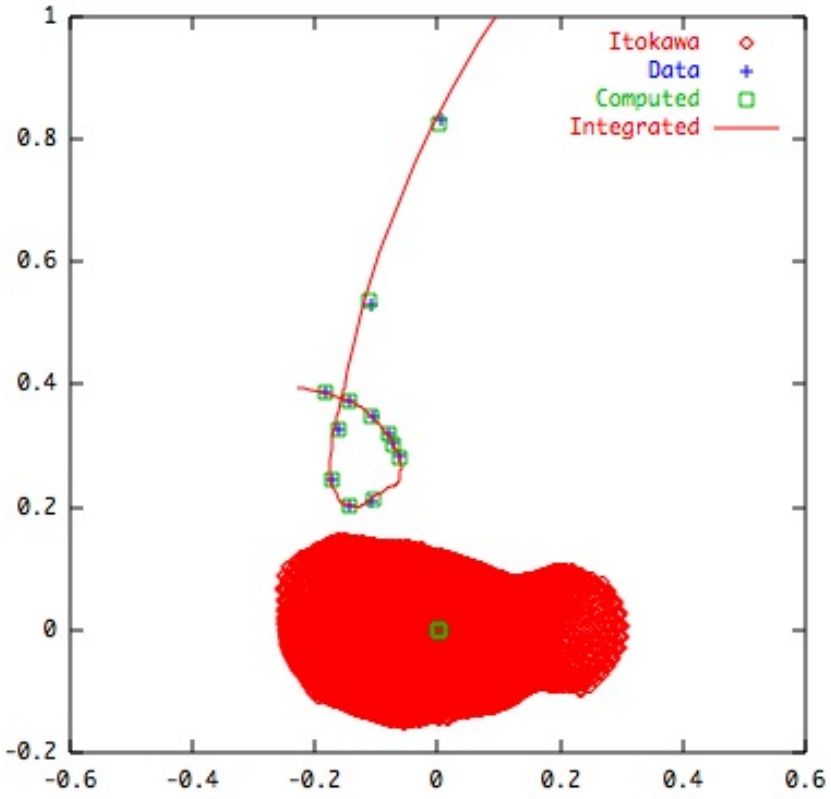

Figure 11. Data points and trajectory during 11/12/05 descent

on these quantities were set relatively tight, meaning that our filter could not move these values very much. The basic model we have for the ith maneuver was:

$$\mathbf{T}_i \quad = \quad \Delta\mathbf{V}_i \delta(t - \tau_i) \tag{6}$$

where $\Delta\mathbf{V}_i$ is the change in velocity, τ_i is the time of the maneuver, and $\delta(t)$ is the Dirac delta function with the properties $\int_{-\infty}^{\infty} \delta(t)dt = 1$ and $\delta(t) = 0$ for $t \neq 0$.

We note that there are also Doppler measurements of the spacecraft during this time period, however they have not been processed as of yet. It is hoped that a future investigation will perform a joint estimation of the asteroid mass distribution using both the optical and the Doppler data. The Doppler data available was used as a consistency check in the current mass determination, to verify that the maneuvers incorporated into the filter were consistent with shifts in the spacecraft line-of-sight velocity.

B. Least-Squares Filter

We used a simple least-squares epoch state filter for our analysis. As the time span considered was short, there was no need to incorporate a more sophisticated filter involving process noise. Additionally, the estimated maneuvers incorporated any effective non-modeled accelerations into our estimation routine. Also, since we only had one measurement type, the difficult issue of relative weighting of different data types was not important.

Given a position measurement $\mathbf{H}_i$ taken at time t_i, and a measurement function $\mathbf{h}(\mathbf{r})$, we form the cost function to be minimized as:

$$J = \frac{1}{2}\sum_{i=1}^{N}(\mathbf{H}_i - \mathbf{h}(\mathbf{r}_i)) \cdot (\mathbf{H}_i - \mathbf{h}(\mathbf{r}_i)) \tag{7}$$

where the position vector $\mathbf{r}_i = \mathbf{r}(t_i; X_o)$ where X_o is the epoch state list of parameters to be estimated. For our case this list includes the position and velocity vectors at epoch, the maneuver Delta-V vectors and the maneuver times, and the total value of $GM = \mu$ for Itokawa. The epoch time was chosen to be prior to the initial measurement by 100 minutes. There should be no physical significance ascribed to the precise values of the epoch position and velocity.

Applying the usual necessary conditions to the cost function for a minimum, $\partial J/\partial X_o = 0$, and assuming that we are close to the true solution, $X_o^* = X_o + \delta X_o$, we find the following set of standard equations to solve for small corrections, δX_o to the current estimate, X_o.

$$\delta X_o = \Lambda^{-1} Z \tag{8}$$

$$Z = \sum_{i=1}^{N}(\mathbf{H}_i - \mathbf{h}_i)\frac{\partial \mathbf{h}_i}{\partial X_o} \tag{9}$$

$$\Lambda = \left[\sum_{i=1}^{N}\frac{\partial \mathbf{h}_i}{\partial X_o}^T \frac{\partial \mathbf{h}_i}{\partial X_o} + P_{XX}^{-1}\right] \tag{10}$$

where P_{XX} is the *a priori* covariance in the estimated parameter list, N is the number of measurements, and all of the measurement functions and partials are evaluated for the current values of the estimated parameter list.

Assuming that the total information matrix, Λ, is invertible a new estimate for the parameters is found as $X_o + \delta X_o$, and is used to recompute the nominal trajectory and all partials. This process is then iterated until the computed corrections are minimal, indicating that the filter has converged upon a solution. In our application of the filter, we then compared the estimated maneuvers and maneuver times with the initial input data to ensure that they did not shift beyond their expected uncertainties.

In practice we were not able to fit all measurements at once, starting from a nominal estimate for the spacecraft position and velocity at epoch. This was due to the highly non-linear trajectory that the spacecraft followed. Rather, we found it necessary to start with a few measurements, converge the trajectory by iteration, and then add the next few measurements to the filter and repeat the process. Proceeding in this way we were able to find an estimated trajectory and associated parameters that fit the measured trajectory closely throughout the time span considered.

C. Variational Equations

At the heart of any filtering process is the computation of the variational equations. For our current system we only needed to compute the partials of the current position vector with respect to the estimated parameter list, or $\partial \mathbf{r}(t; X_o)/\partial X_o$. However, it is simpler to discuss the more general partial of the current state, $\mathbf{r}, \mathbf{v}$, with respect to the parameter list, where $\mathbf{v} = \dot{\mathbf{r}}$. For ease of presentation we will only consider the truncated parameter list: $X = [\mathbf{r}_o, \mathbf{v}_o, \mu, \Delta\mathbf{V}, \tau]$, where the o sub-script denotes the position and velocity at the epoch time.

The variational matrix is then specified as:

$$\frac{\partial(\mathbf{r}, \mathbf{v})}{\partial X_o} = \Phi \tag{11}$$

$$= \begin{bmatrix} \Phi_{rr_o} & \Phi_{rv_o} & \Phi_{r\mu} & \Phi_{r\Delta V} & \Phi_{r\tau} \\ \Phi_{vr_o} & \Phi_{vv_o} & \Phi_{v\mu} & \Phi_{v\Delta V} & \Phi_{v\tau} \end{bmatrix} \tag{12}$$

where $\Phi_{rr_o} = \frac{\partial \mathbf{r}}{\partial \mathbf{r}_o}$, etc. The variational matrix Φ is found by integrating the following time-varying linear dynamics equations evaluated along the nominal trajectory:

$$\dot{\phi} = A\phi \tag{13}$$

$$\phi = \begin{bmatrix} \Phi_{rr_o} & \Phi_{rv_o} \\ \Phi_{vr_o} & \Phi_{vv_o} \end{bmatrix} \tag{14}$$

$$A = \begin{bmatrix} 0_{3x3} & I_{3x3} \\ -\omega^2 \tilde{\mathbf{z}}\tilde{\mathbf{z}} + U_{\mathbf{rr}} & -2\omega\tilde{\mathbf{z}} \end{bmatrix} \tag{15}$$

$$\tag{16}$$

with initial conditions $\phi(t_o, t_o) = I_{6x6}$. The remaining equations are reduced to non-homogeneous linear equations:

$$\begin{bmatrix} \dot{\Phi}_{r\mu} \\ \dot{\Phi}_{v\mu} \end{bmatrix} = A \begin{bmatrix} \Phi_{r\mu} \\ \Phi_{v\mu} \end{bmatrix} + \begin{bmatrix} 0_{3x1} \\ \frac{1}{\mu} U_{\mathbf{r}} \end{bmatrix} \tag{17}$$

$$\begin{bmatrix} \dot{\Phi}_{r\Delta V} \\ \dot{\Phi}_{v\Delta V} \end{bmatrix} = A \begin{bmatrix} \Phi_{r\Delta V} \\ \Phi_{v\Delta V} \end{bmatrix} + \begin{bmatrix} 0_{3x3} \\ I_{3x3}\delta(t-\tau) \end{bmatrix} \tag{18}$$

$$\begin{bmatrix} \dot{\Phi}_{r\tau} \\ \dot{\Phi}_{v\tau} \end{bmatrix} = A \begin{bmatrix} \Phi_{r\tau} \\ \Phi_{v\tau} \end{bmatrix} + \begin{bmatrix} 0_{3x1} \\ \Delta\mathbf{V}\frac{\partial\delta(t-\tau)}{\partial\tau} \end{bmatrix} \tag{19}$$

all with zero initial conditions. In the above 0_{nxm} and I_{nxm} stand for the n by m zero and identity matrix, respectively, and

$$\tilde{\mathbf{z}} = \begin{bmatrix} 0 & -1 & 0 \\ 1 & 0 & 0 \\ 0 & 0 & 0 \end{bmatrix} \tag{20}$$

The entire computation is straight-forward, except for handling the Dirac delta function and its partial. First recall the standard solution for the non-homogenous linear differential equation for a vector χ with zero initial conditions, $\chi_o = 0$:

$$\dot{\chi} = A\chi + B(t) \tag{21}$$

$$\chi(t, t_o) = \phi(t, t_o) \int_{t_o}^{t} \phi(t_o, t') B(t') dt' \tag{22}$$

$$\phi^{-1}(t, t_o) = \phi(t_o, t) \tag{23}$$

Carefully going through the derivation, and properly incorporating the Dirac delta function, we find the following result for the partial with respect to $\Delta\mathbf{V}$:

$$\begin{bmatrix} \Phi_{r\Delta V} \\ \Phi_{v\Delta V} \end{bmatrix} = \begin{cases} 0_{6x1} & t < \tau \\ \phi(t, \tau) \begin{bmatrix} 0_{3x3} \\ I_{3x3} \end{bmatrix} & t \geq \tau \end{cases} \tag{24}$$

For the partial with respect to τ we note that, from the fundamental rule of calculus, the time integral of the partial of $\delta(t)$ with respect to t must equal $\delta(t)$. We also note the special structure between the position partial and the velocity partial, and that the other terms in the equations can be ignored when around $t = \tau$. This allows us to define the approximate result:

$$\ddot{\Phi}_{r\tau} = \Delta\mathbf{V}\frac{\partial\delta(t-\tau)}{\partial\tau} \tag{25}$$

Integrating twice with respect to time around the epoch $t = \tau \pm \epsilon$, $\epsilon \ll 1$ yields:

$$\Phi_{r\tau} = -\Delta\mathbf{V} \tag{26}$$

$$\Phi_{v\tau} = 0_{3x1} \tag{27}$$

which allows us to propagate the solution forward in time to find:

$$\begin{bmatrix} \Phi_{r\tau} \\ \Phi_{v\tau} \end{bmatrix} = \begin{cases} 0_{6x1} & t < \tau \\ \phi(t,\tau) \begin{bmatrix} -\Delta\mathbf{V} \\ 0_{3x1} \end{bmatrix} & t \geq \tau \end{cases} \tag{28}$$

D. Data and Measurement Partials

The main data that was processed in this mass determination were expressed as position vectors of the spacecraft in the asteroid-fixed frame at specified epochs. The methodology used in determining these relative position vectors is described in (Gaskell et al. 2006b), and includes the processing of optical imagery, lidar measurements, and the construction of a detailed photoclinometry map of the body, which can generate a shape model of the body. The fact that the measurements were taken and specified in the same frame used for the dynamics modeling greatly simplified the derivation and coding of the filter. Specifically, the measurement function for these data is just the position vector of the spacecraft, with the partials with respect to the epoch state following simply:

$$\mathbf{h}(\mathbf{r}) = \mathbf{r}(t) \tag{29}$$

$$\frac{\partial \mathbf{h}}{\partial \mathbf{r}_o} = \Phi_{rr_o}(t,t_o) \tag{30}$$

$$\frac{\partial \mathbf{h}}{\partial \mathbf{v}_o} = \Phi_{rv_o}(t,t_o) \tag{31}$$

$$\frac{\partial \mathbf{h}}{\partial \Delta\mathbf{V}_i} = \Phi_{r\Delta V_i}(t,t_o) \tag{32}$$

$$\frac{\partial \mathbf{h}}{\partial \tau_i} = \Phi_{r\tau_i}(t,t_o) \tag{33}$$

$$\frac{\partial \mathbf{h}}{\partial \mu} = \Phi_{r\mu}(t,t_o) \tag{34}$$

which were all discussed previously.

Due to the simple form of the measurement function, the partials of measurements with respect to the other estimated states of asteroid mass, maneuver delta-V's and maneuver times only involved the variational equations for the spacecraft trajectory.

E. Results

Using the described data, model and filter we estimated the total Itokawa gravitational parameter to be:

$$\mu = (2.36 \pm 0.15) \times 10^{-9} \text{ km}^3/\text{s}^2 \tag{35}$$

The quoted error is the formal 1-σ error for assuming a measurement accuracy of 10 meters. The residuals are shown in Fig. 12, where we note that they are all much less than 10 meters. The estimated shifts in the maneuver times were all less than 13 seconds, with most less than 5 seconds, and the shift in absolute magnitude were all less than 2 mm/s, near the noise limit for the thrusters.

It is also illustrative to look at the orbit elements during the data span, shown in Figs. 13 - 15. There we note the clear presence of maneuvers during the arc, apparent when the elements have an abrupt change. Of most interest is the closest approach portion between 2.5 and 3 hours. We first note the absence of maneuvers during a portion of that arc. We next note the strong variation in the orbit elements during that period – indicating that the spacecraft trajectory was being substantially perturbed by the rotating gravity field. If there had been no maneuvers performed around this closest approach portion, and if additional optical navigation images had been available for measurements, a much more precise estimate of the asteroid mass would have resulted.

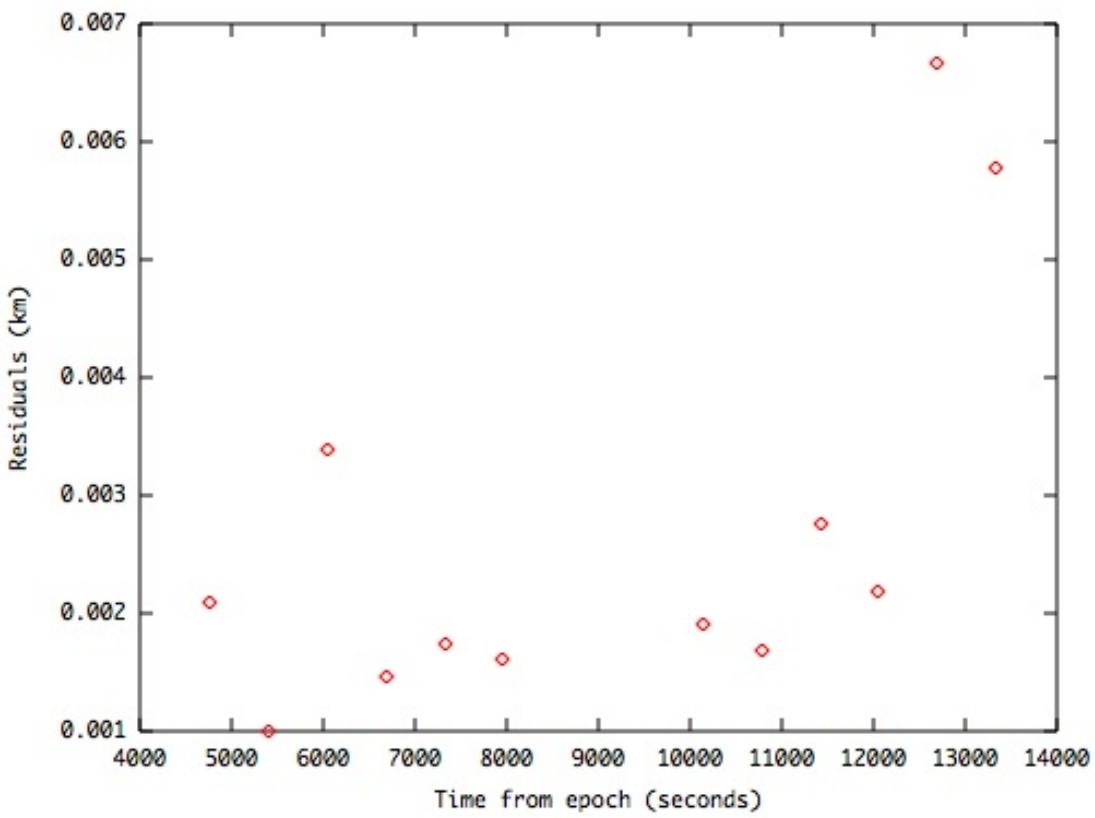

Figure 12. Residuals between the computed measurements and the actual measurements. The computed and measured position vectors at the measurement time are differenced and their magnitude taken. We note that the residuals are all less than 10 meters. The semi-major axis and eccentricity are not plotted after the trajectory becomes hyperbolic.

V. Conclusions

A study of the dynamical environment about Asteroid 25143 Itokawa, the target of the Japanese space mission Hayabusa, is given based on the measured shape and mass obtained during the Hayabusa spacecraft's period of close proximity. In addition a detailed discussion of one method used for determining the mass of the asteroid is described and results given.

Acknowledgements

DJS acknowledges the support of a fellowship from the Japan Society for the Promotion of Science.

Appendix

Following are the Itokawa gravity coefficients through order 4 (shown in Table I). These coefficients are normalized, as defined in Kaula (2000), computed with respect to a normalizing radius $R_s = 0.161915$ km.

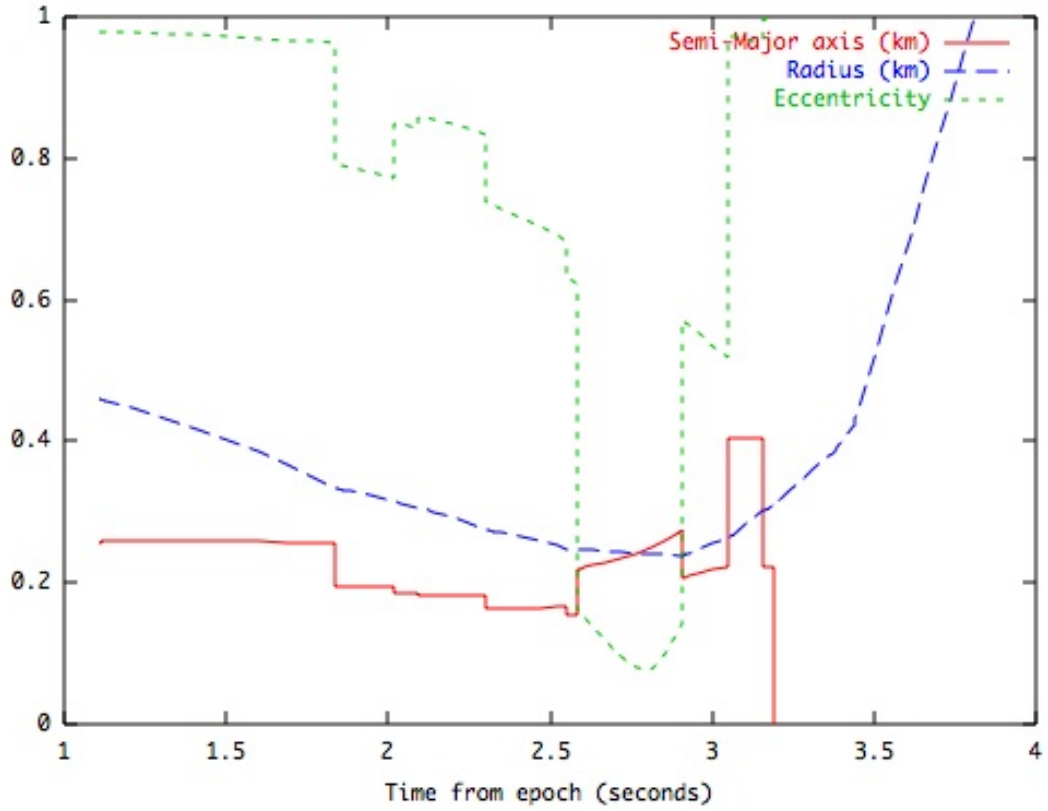

Figure 13. Orbit elements of Semi-major axis and eccentricity during the measurement span. The radius of the spacecraft is also shown. Note the large change in eccentricity during the ballistic portion prior to closest approach.

The general form of the gravitational field can be expressed as:

$$U = \sum_{l=0}^{\infty} \sum_{m=0}^{l} \left(\frac{R_s}{r}\right)^{l+1} P_{lm}(\sin\phi) \left[C_{lm}\cos m\lambda + Slm \sin m\lambda\right], \tag{36}$$

where P_{lm} are the normalized Legendre polynomials, ϕ is the particle latitude, and λ is the particle longitude in the body-fixed frame.

Bibliography

Abe, S., T. Mukai, N. Hirata, O. S. Barnouin-Jha, A. F. Cheng, H. Demura, R. W. Gaskell, T. Hashimoto, K. Hiraoka, T. Honda, T. Kubota, M. Matsuoka, T. Mizuno, R. Nakamura, D.J. Scheeres, M. Yoshikawa. 2006. "Mass and Local Topography measurements of Itokawa by Hayabusa," *Science* 312: 1344-1347.

Demura, H., S. Kobayashi, E. Nemoto, N. Matsumoto, M. Furuya, A. Yukishita, N. Muranaka, H. Morita, K. Shirakawa, M. Maruya, H. Ohyama, M. Uo, T. Kubota, T. Hashimoto, J. Kawaguchi, A. Fujiwara, J. Saito, S. Sasaki, H. Miyamoto, N. Hirata. 2006. "Pole and Global Shape of (25143) Itokawa," *Science* 312: 1347–1349.

Fujiwara, A., J. Kawaguchi, D. K. Yeomans, M. Abe, T. Mukai, T. Okada, J. Saito, H. Yano, M.

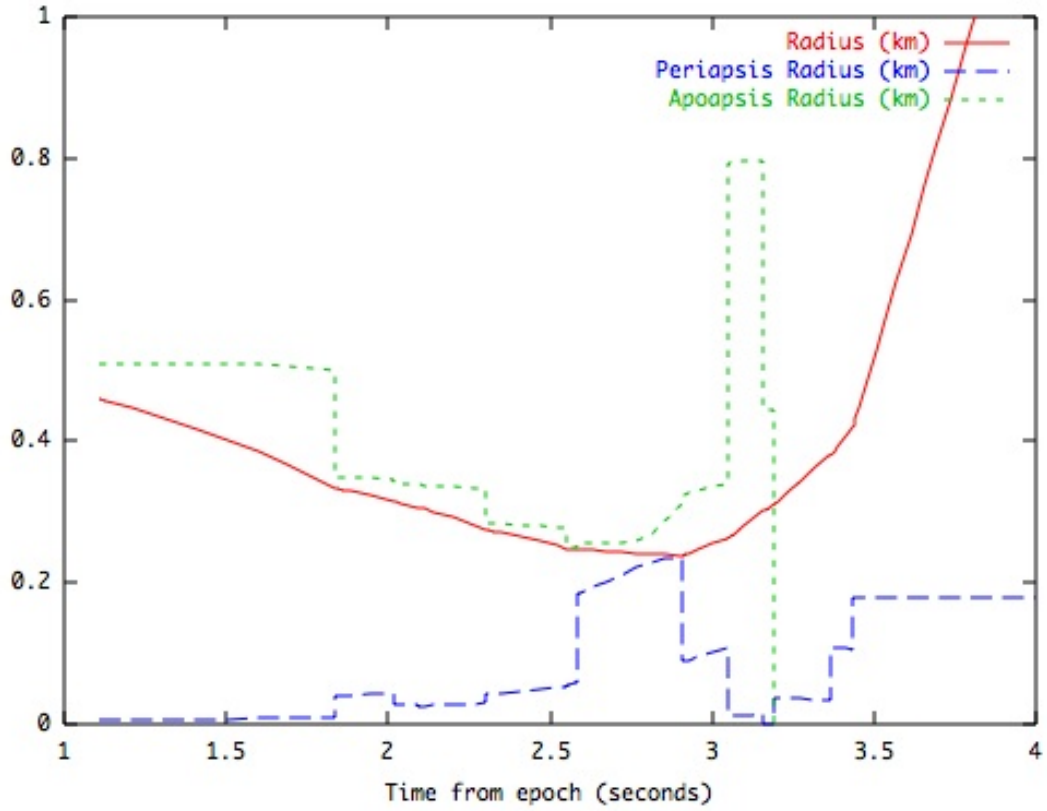

Figure 14. Apoapsis, periapsis and radius of the spacecraft during the measurement span. Note the large change in periapsis radius during the ballistic portion prior to closest approach. The Apoapsis radius is not plotted after the trajectory becomes hyperbolic.

Yoshikawa, D. J. Scheeres, O. Barnouin-Jha, A. F. Cheng, H. Demura, R. W. Gaskell, N. Hirata, H. Ikeda, T. Kominato, H. Miyamoto, A. M. Nakamura, R. Nakamura, S. Sasaki, and K. Uesugi. 2006. "The Near-Earth Asteroid ITOKAWA observed by Hayabusa: Its Possible Structure and History," *Science* 312: 1330–1334.

Gaskell R., Saito J., Ishiguro M., Kubota T., Hashimoto T., Hirata N., Abe S., Barnouin-Jha O., Scheeres D. "Global Topography of Asteroid 25143 Itokawa," Lunar and Planetary Science XXXVII meeting, Houston, Texas, March 2006, Abstract #1876.

Gaskell, R.W., O. Barnouin-Jha, D. Scheeres, T. Mukai, N. Hirata, S. Abe, J. Saito, M. Ishiguro, T. Kubota. Yoshikawa, K. Shirakawa, T. Kominato, "Landmark Navigation Studies and Target Characterization in the Hayabusa Encounter with Itokawa," Astrodynamics Specialist Conference, Keystone, Colorado, August 2006.

Hu, W. and D.J. Scheeres. 2004. "Numerical Determination of Stability Regions for Orbital Motion in Uniformly Rotating Second Degree and Order Gravity Fields," Planetary and Space Science 52: 685-692.

Kaula, W.M. 2000. *Theory of Satellite Geodesy*, Dover Publishing.

Kubota, T., Hashimoto, T., Uo, M., Maruya, M., and Baba, K., "Maneuver Strategy for Station Keeping and Global Mapping around an Asteroid," Space- flight Mechanics 2001: Advances in the Astronautical Sciences, Vol. 108, 2001, pp. 769-779, AAS Paper 01-156.

Lee, P. 1996. Icarus 124: 181-194.

Miller, J.K., A.S. Konopliv, P.G. Antreasian, J.J. Bordi, S. Chesley, C.E. Helfrich, W.M. Owen, T.C. Wang, B.G. Williams, D.K. Yeomans, and D.J. Scheeres. 2002. "Determination of shape, gravity and

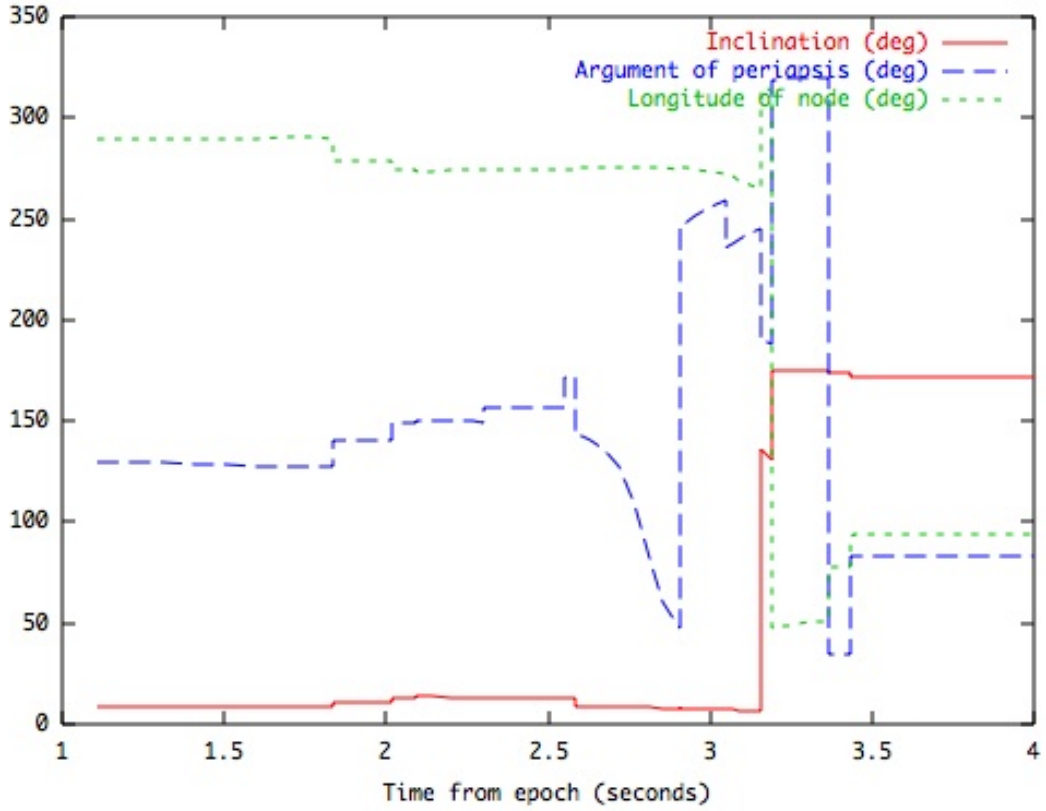

Figure 15. Inclination, argument of periapsis and longitude of the ascending node of the spacecraft during the measurement span. Note the large change in argument of periapsis during the ballistic portion prior to closest approach.

rotational state of Asteroid 433 Eros," *Icarus* 155: 3-17.

Robinson, M.S., P.C. Thomas, J. Veverka, S. Murchie, and B. Carcich 2001. Nature 413: 396–399.

Scheeres, D.J. 1994. "Dynamics About Uniformly Rotating Tri-Axial Ellipsoids. Applications to Asteroids," Icarus 110:225-38.

Scheeres, D.J., S.J. Ostro, R.S. Hudson, and R.A. Werner. 1996. "Orbits Close to Asteroid 4769 Castalia," Icarus 121:67-87.

Scheeres, D.J. 1999. "Satellite Dynamics about small bodies: Averaged Solar Radiation Pressure Effects," Journal of the Astronautical Sciences 47:25-46.

Scheeres, D.J., B.G.Williams, and J.K. Miller. 2000. "Evaluation of the Dynamic Environment of an Asteroid: Applications to 433 Eros," Journal of Guidance, Control and Dynamics 23:466-475.

Scheeres, D.J. and F. Marzari. 2002. "Spacecraft dynamics in the vicinity of a comet," Journal of the Astronautical Sciences 50(1): 35-52.

Werner, R.A. and D.J. Scheeres. 1997. "Exterior Gravitation of a Polyhedron Derived and Compared with Harmonic and Mascon Gravitation Representations of Asteroid 4769 Castalia," *Celestial Mechanics and Dynamical Astronomy* 65:313–44.

Werner, R.A., 1997. Spherical harmonic coefficients for the potential of a constant-density polyhedron. Comput. & Geosci. 23, 1071.

Yano, H., T. Kubota, H. Miyamoto, T. Okada, D. J. Scheeres, Y. Takagi, K. Yoshida, M. Abe, S. Abe, O. Barnouin-Jha, A. Fujiwara, S. Hasegawa, T. Hashimoto, M. Ishiguro, M. Kato, J. Kawaguchi, T. Mukai,

Table 1. Itokawa normalized gravity field coefficients through degree and order 4 for a constant density gravity field. A gravity field through degree and order 16 is available from the authors. Definition of the normalization constants can be found in Kaula (2000).

Order l	Degree m	C Coefficient C_{lm}	S Coefficient S_{lm}
0	0	1.0	–
1	0	0.0	–
1	1	0.0	0.0
2	0	-0.145216	–
2	1	0.0	0.0
2	2	0.219420	0.0
3	0	0.036115	–
3	1	-0.028139	-0.006137
3	2	-0.046894	-0.046894
3	3	0.069022	0.033976
4	0	0.087852	–
4	1	0.034069	0.004870
4	2	-0.123263	0.000098
4	3	-0.030673	-0.015026
4	4	0.150282	0.011627

J. Saito, S. Sasaki, and M. Yoshikawa. 2006. "Touch-down of the Hayabusa spacecraft at the Muses Sea on Itokawa," *Science* 312: 1350-1353.

Yoshikawa, M., H. Ikeda, H. Yano, J. Saito, T. Kubota, T. Hashimoto, A. Fujiwara, J. Kawaguchi, T. Kominato, M. Matsuoka, K. Shirakawa, T. Ohnishi, S. Abe, T. Mukai, R. Gaskell, and D.J. Scheeres, "Astrodynamics Science about Itokawa, Gravity and Ephemeris," Astrodynamics Specialist Conference, Keystone, Colorado, August 2006.